Accepted Manuscript

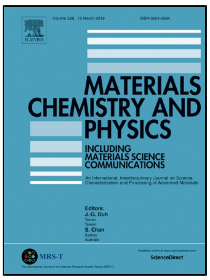

Microstructural characterization and modified spectral response of cobalt doped NiO nanoparticles

P.A. Sheena, H. Hitha, A. Sreedevi, Thomas Varghese

PII:	S0254-0584(19)30233-0
DOI:	10.1016/j.matchemphys.2019.03.033
Reference:	MAC 21472
To appear in:	*Materials Chemistry and Physics*
Received Date:	31 August 2018
Accepted Date:	09 March 2019

Please cite this article as: P.A. Sheena, H. Hitha, A. Sreedevi, Thomas Varghese, Microstructural characterization and modified spectral response of cobalt doped NiO nanoparticles, *Materials Chemistry and Physics* (2019), doi: 10.1016/j.matchemphys.2019.03.033

Microstructural characterization and modified spectral response of cobalt doped NiO nanoparticles

P. A. Sheena[a,b,c], H. Hitha[c], A. Sreedevi[c], Thomas Varghese[c]
[a]Department of Physics, M.E.S. Asmabi College, P. Vemballur-680 671, Kerala, India
[b]Department of Physics, Newman College, Thodupuzha-685584, Kerala, India
[c]Nanoscience research centre (NSRC), Department of Physics, Nirmala College, Muvattupuzha-686661, Kerala, India

Abstract

The modifications in the microstructure and optical properties of cobalt doped nickel oxide nanoparticles *($Ni_{1-x}Co_xO$,* x= 0, 0.01, 0.03, 0.05 and 0.10) synthesized by co-precipitation method is reported here. X-ray diffraction, field emission electron microscope, energy dispersive X-ray spectroscopy, and high resolution transmission electron microscopy techniques reveal successful incorporation of *Co* into the NiO lattice without compromising its intrinsic structure. X-ray photoelectron spectroscopy analysis confirms the compositional purity of the sample. The bandgap tuning of NiO is achieved by *Co* doping as confirmed by UV–visible absorption studies. Significant variation is observed in the luminescence intensity with *Co* doping. Surface oxygen vacancies and defects play a pivotal role in controlling the emission properties of NiO. This is the first report on the enhancement of PL intensity with *Co* doping of NiO nanoparticles. The modified spectral response of *Co* doped NiO is expected to have various optoelectronic applications.

Keywords: *Co* doped NiO, microstrain, optical bandgap, oxygen vacancies

1. Introduction

Nanoscale transition metal oxides are gaining considerable attention owing to their excellent performance in various applications. Among them, nickel oxide (NiO) has attracted considerable research interest due to its low cost, durability, excellent electrochemical stability and various manufacturing possibilities [1]. It is one of the very few p-type semiconducting oxides with a wide bandgap in the range of 3.6 – 4 eV [2]. It is a promising metal oxide for many applications such as electrochromic displays [3], gas sensors [4], catalysis [5], magnetic materials [6], anode material in Li ion batteries [7] and dye-sensitized solar cell (DSSC) technologies [8]. But, its low valence band edge restricts the wide use of NiO in DSSCs [9]. Unfortunately the large bandgap has restricted its applications only into the harmful and expensive ultra violet region. The efficiency of NiO as a light absorber in photovoltaic applications is greatly reduced, as it is virtually inactive in the visible region. Therefore, tailoring of the bandgap is essential for modifying the properties of NiO for optoelectronic device applications.

Doping is the primary technique used to control the properties of nanostructured semiconductors and to obtain new materials of technological importance [10]. The introduction of impurities can create defects in the host lattice, thereby changing its optical, magnetic and electrical properties. The doping of transition metal elements like cobalt and zinc at the nickel site can strongly modify the optical properties of NiO. The high solubility and abundant electron states make cobalt (*Co*) a promising dopant in NiO systems [11]. As *Co* is a good luminescence activator, it can also modify the emission properties of NiO [12]. The lattice parameters of nickel oxide and cobalt oxide, both having rock salt structure are 4.195 and 4.261 Å, respectively. Also the crystal ionic radius of *Ni* (0.69 Å) is comparable with that of *Co* (0.74 Å) [13]. Hence, NiO can be doped with relatively high amount of *Co* without causing much lattice strain. A few reports are available on the studies of *Co* doped NiO nanoparticles. Natu *et al*. reported the lowering of Fermi level of NiO thin film with cobalt doping which makes them suitable for p-type DSSCs [14]. The optical bandgap of NiO is found to decrease with *Co* doping as reported by Taşkopru *et al.* [15]. Agarwal *et al.* reported a decrease in the emission intensity of NiO on *Co* doping [16]. However, no reports cover a detailed investigation of effect of *Co* doping on structural and optical properties of NiO nanoparticles. To bridge the existing gap in the reported literature, we report detailed microstructural and optical studies of pristine and cobalt doped NiO nanoparticles. Compared to other reports, significant reduction in crystallite size is obtained in the present study.

Several techniques have been used for the synthesis of pristine and doped NiO nanostructures such as sol-gel [17], co-precipitation [18], hydrothermal [19], solvo-thermal [20] and chemical precipitation [21, 22]. Among them, the preparation of pure and cobalt-doped NiO nanostructures through chemical co-precipitation can control the crystallite size and morphology of the samples [23]. NiO nanoparticles doped with low, intermediate and high dopant levels (1, 3, 5 and 10 mol %) of cobalt through chemical co-precipitation method are chosen for the present study.

In the present work, *NiO* nanoparticles doped with different dopant levels of *Co* are synthesized through chemical co-precipitation method. The synthesized samples are structurally characterized by X-ray diffraction (XRD), field emission scanning electron microscope (FESEM), energy dispersive X-ray spectroscopy (EDAX), X-ray photoelectron spectroscopy (XPS), high resolution transmission electron microscopy (HRTEM) and Fourier transform infrared (FTIR) spectroscopy. Optical properties of the samples are investigated using UV – Visible absorption and photoluminescence (PL) spectroscopic techniques. These

systematic studies elucidate new results for potential applications and stand the first comprehensive report.

2. Experimental

All chemicals used in this experiment are of analytical grade. Nickel nitrate hexahydrate (Ni $(NO_3)_2 \cdot 6H_2O$, 99.8%, Sigma Aldrich), Ammonium carbonate ($(NH_4)_2CO_3$, 99.9%, Merck), Cobalt nitrate hexahydrate (Co $(NO_3)_2.6H_2O$, 99.8%, Sigma Aldrich) are used for the synthesis of the samples.

2.1 Synthesis

In the present work, pristine and cobalt doped NiO nanoparticles with 1, 3, 5 and 10 mol % of doping are prepared by chemical co-precipitation method [24]. To synthesize NiO nanoparticles, 0.1 M solution of nickel nitrate hexahydrate [Ni $(NO_3)_26H_2O$] is prepared at room temperature. The carbonate precursor is chemically precipitated by slowly adding 0.1 M aqueous solution of ammonium carbonate [$(NH_4)_2CO_3$] at room temperature under magnetic stirring for 30 minutes. The precipitate is allowed to settle down overnight and then washed several times with distilled water to remove the unreacted salts and impurities. Finally the precipitate is filtered and dried in a hot air oven at 70^{o}C for 18 h. The dried product obtained is powdered and calcined at 400^{o}C for 3 h in a muffle furnace to obtain NiO nanoparticles. The same procedure is followed for the synthesis of *Co* doped NiO samples, with the addition of stoichiometric amounts of cobalt nitrate hexahydrate [Co $(NO_3)_2.6H_2O$]. The synthesized pristine NiO nanoparticles and 1, 3, 5 and 10 mol % *Co* doped NiO nanoparticles are denoted as C0, C1, C3, C5 and C10 respectively.

2.2 Characterization Techniques

The structure and phase purity of the prepared samples are identified using Bruker D8 Advance X-ray diffractometer with Cu-Kα as the radiation source of wavelength 1.5406 Å. The samples are scanned in the range of 30 – 90^o, at the rate of 0.005^o/s and step size of 0.02^o. Field emission scanning electron microscope and energy dispersive X-ray spectroscopy attached with the FESEM equipment (Ultra Plus, ZEISS) is utilized for the micro structural and compositional analyses of the samples. The morphology of pristine and doped samples is analyzed by JEOL-3010 high resolution transmission electron microscope. The elemental composition of the sample is studied by X-ray photoelectron spectroscopy (PerkinElmer 590/550 A). The IR spectra are recorded by a Fourier transform infrared spectrophotometer (Perkin Elmer Spectrum 100).

The optical absorption spectra of the samples are obtained from a Shimadzu 2600/2700 UV - Visible spectrophotometer in the wavelength range of 200–800 nm. Photoluminescence spectrum is recorded using Fluoromax 3 spectrophotometer using 280 nm as excitation wavelength at room temperature.

3. Results and Discussion

3.1 XRD Analysis

The powder X-ray diffraction patterns of pure and *Co* doped NiO nanoparticles calcined at 400^{o}C are shown in Fig. 1. All the diffraction peaks of both pristine and doped samples are well indexed with the standard JCPDS Card no. (73-1519). All patterns exhibit a cubic structure with a preferential orientation along (200) plane without any additional impurity phase, indicating that the structure is not affected by *Co* substitution. The peaks corresponding to (111), (200), (220), (311), and (222) planes confirmed the formation of face-centred cubic (fcc) structure with space group *Fm3m* [25]. For all dopant concentrations, no evidence of secondary phases or phases other than that of NiO is found which indicates that the *Co* dopant get substituted at the *Ni* site without affecting the cubic structure. Only slight shift in the peaks is observed in the doped samples which confirm substitutional doping. In addition, a decrease in the intensity of diffraction peaks is observed with an increase in doping concentration, indicating a loss of crystallinity and decrease in crystal symmetry due to lattice distortion. This suggests an increase in micro strain due to disorder in the crystalline structure with *Co* doping [26]. The average crystallite size of the samples calculated using Scherrer equation [27] is found to be 9.7, 7.7, 7, 7.5 and 8.2 nm respectively for C0, C1, C3, C5 and C10 samples. The crystallite size is found to decrease with increase in doping concentration up to 3 mol %, but shows an increasing trend thereafter. This indicates that for lower doping concentrations, substitutional replacement of *Ni* with Co^{2+}ions may occur. However at higher doping, the dopant ions enter into the interstitial sites of NiO lattice [28].

The size (D) and microstrain (ε) contribution to XRD peak broadening could be obtained from the full-width at-half-maximum (FWHM) of the diffraction peaks using Hall-Williamson relation [29],

$$\beta\cos\theta = k\lambda/D + 4\varepsilon\sin\theta. \quad (1)$$

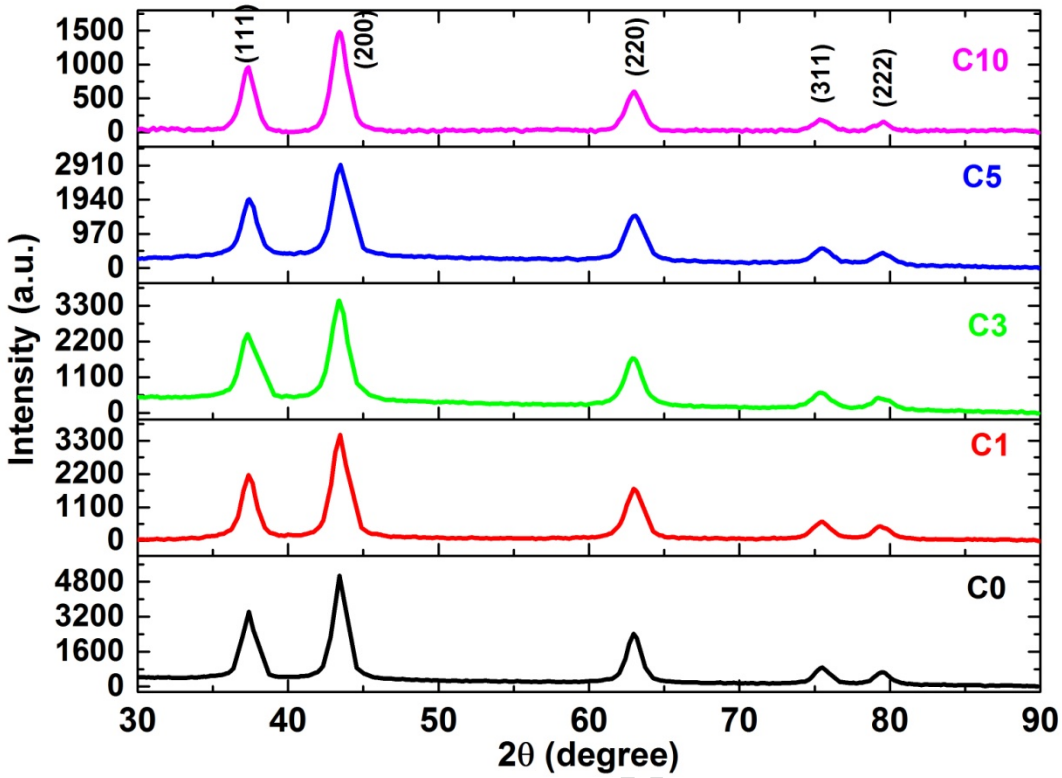

Fig.1 XRD patterns of NiO and *Co* doped NiO nanoparticles

The slope of the straight line graph (Fig.2) obtained by plotting (βcosθ) *vs* (4sinθ) gives the microstrain ε, while the average crystallite size corrected for microstrain is obtained from the y-intercept. Geometric parameters of NiO nanoparticles obtained from XRD results are presented in Table 1. The table confirms that the crystallite size estimated from Williamson-Hall plot matches with that calculated using Scherrer equation. The microstrain is found to increase with doping, as expected. The comparatively large values of microstrain for the C5 and C10 samples confirm the interstitial incorporation of *Co* ions, as discussed.

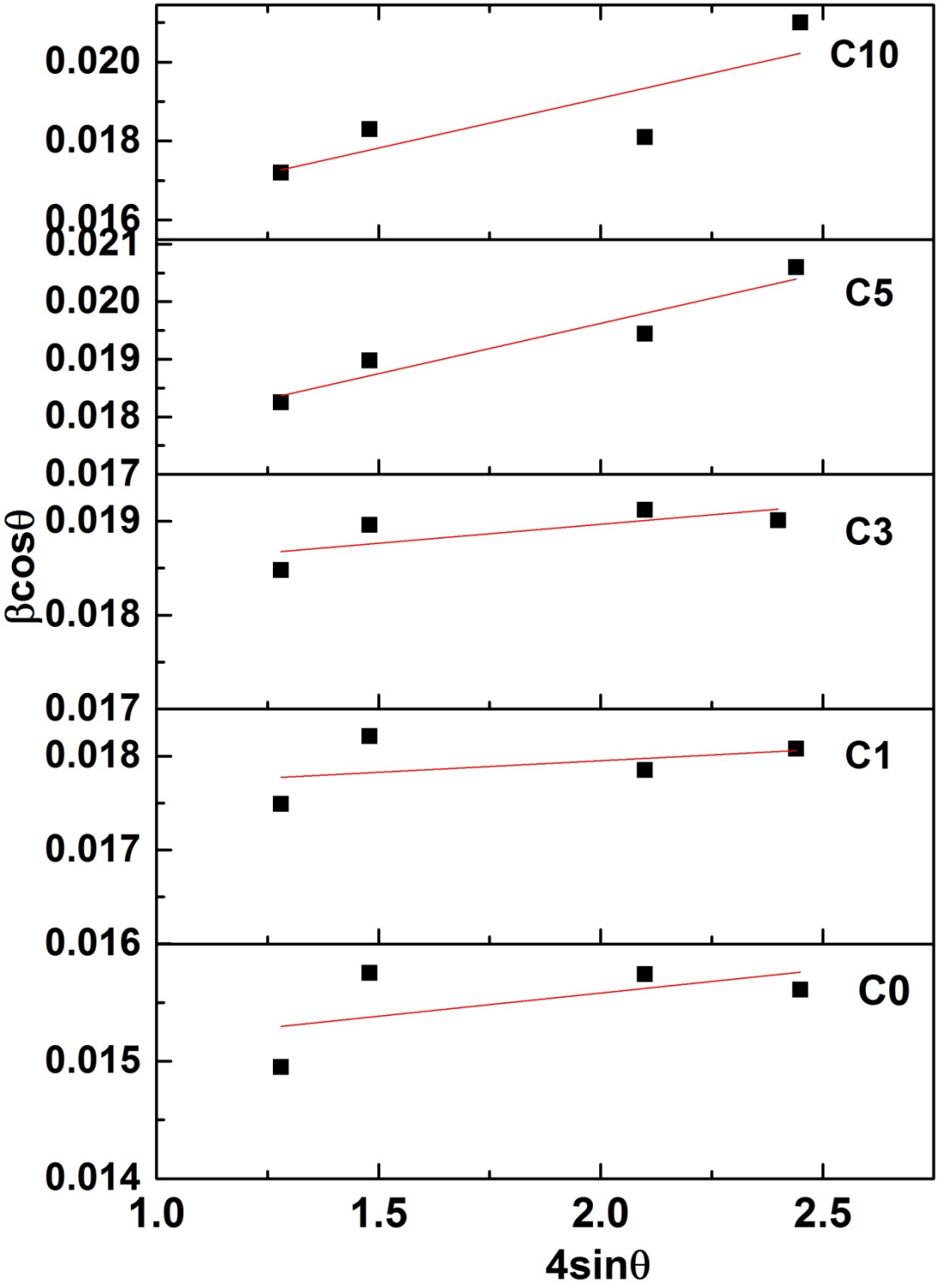

Fig.2 W – H plot of NiO and *Co* doped NiO nanoparticles

Table 1. Geometric parameters of pure and *Co* doped NiO samples from XRD spectra

Sample	FWHM of (200) peak	d spacing of {200} planes	Crystallite size (nm)		Microstrain
			Scherrer equation	W-H analysis	
C0	**0.972**	**0.2088**	**9.7±0.19**	**9.30±0.186**	**3.95x 10^{-4}**
C1	**1.086**	**0.2081**	**7.7±0.15**	**7.90±0.158**	**2.454x 10^{-4}**
C3	**1.229**	**0.209**	**7.0±0.14**	**7.55±0.151**	**4.035x 10^{-4}**
C5	**1.170**	**0.2083**	**7.5±0.15**	**8.50±0.170**	**17.5x 10^{-4}**
C10	**1.129**	**0.2079**	**8.2±0.16**	**9.80±0.196**	**25.3x 10^{-4}**

3.2 FTIR Studies

In order to understand the chemical bonds and molecular structure of the samples, FTIR spectra are recorded. Fig.3 shows the FTIR spectra of pure and *Co* doped NiO samples in the range 400 to 4000 cm^{-1}. The absorption band centred at 415 cm^{-1} is assigned to Ni–O stretching vibration mode [30]. The broad absorption band centered at 3427 cm^{-1} is assigned to O-H stretching vibration and the band at 1630 cm^{-1} is attributable to H-O-H bending vibration mode [25, 31]. The sharp peak located at 1383 cm^{-1} is due to atmospheric CO_2 absorption [32]. No additional absorption peaks are observed in the spectrum with the addition of *Co*, which indicates the homogeneous dispersion of the dopant in the host material. This is in accordance with the XRD results.

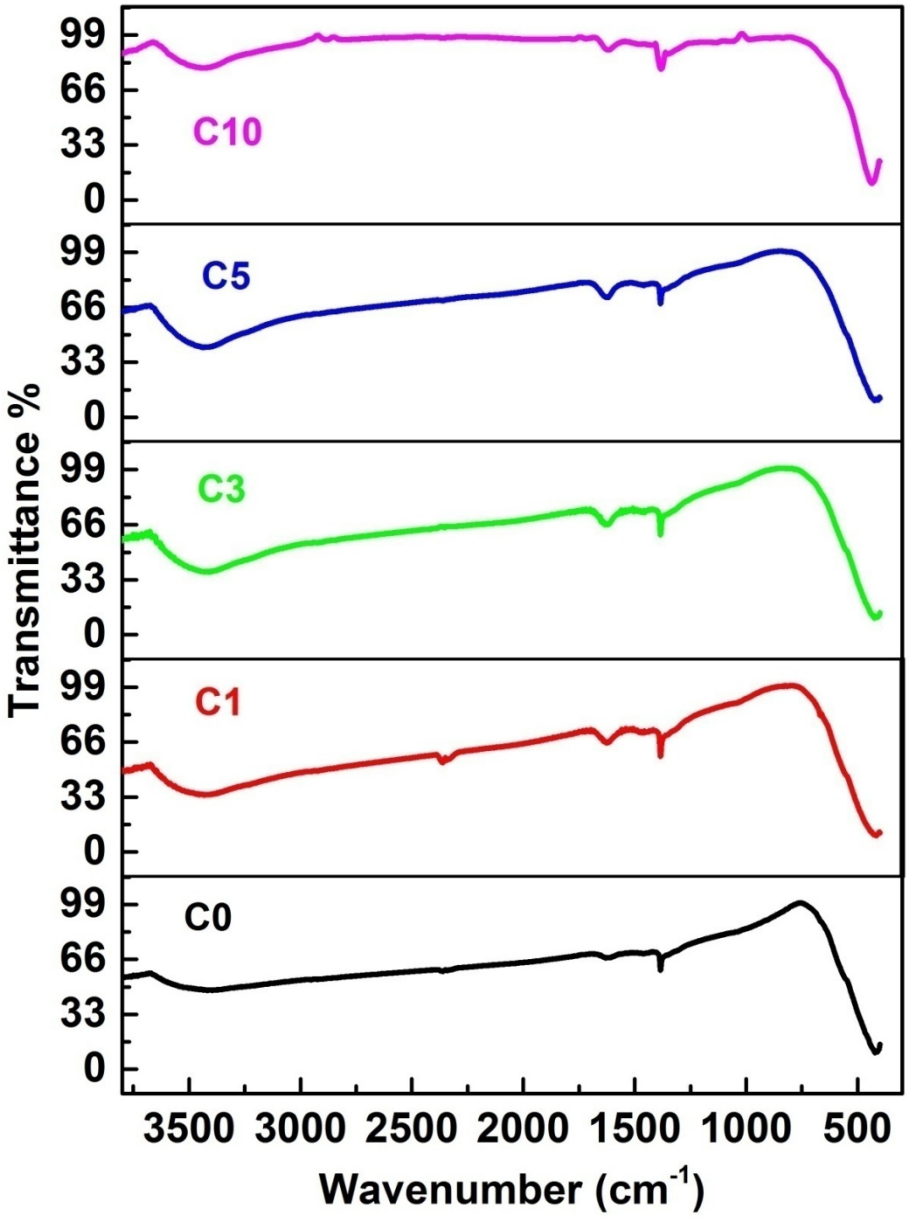

Fig.3 FTIR spectra of NiO and *Co* doped NiO nanoparticles

3.3 Electron Microscopy

3.3.1 FESEM and EDAX

The surface morphology of pure and *Co* doped NiO nanoparticles are studied by FESEM analysis. The FESEM images of pristine and doped samples are shown in Fig. 4. The images show non-spherical particles with uniform size. The uniform grain distribution as seen in the images confirms complete incorporation of *Co* in the NiO lattice. Aggregation of particles is observed for all the samples, which may be due to their small crystallite size. The

nanoparticles have a tendency to agglomerate in order to minimize the high surface energy caused by the high surface area to volume ratio [26].

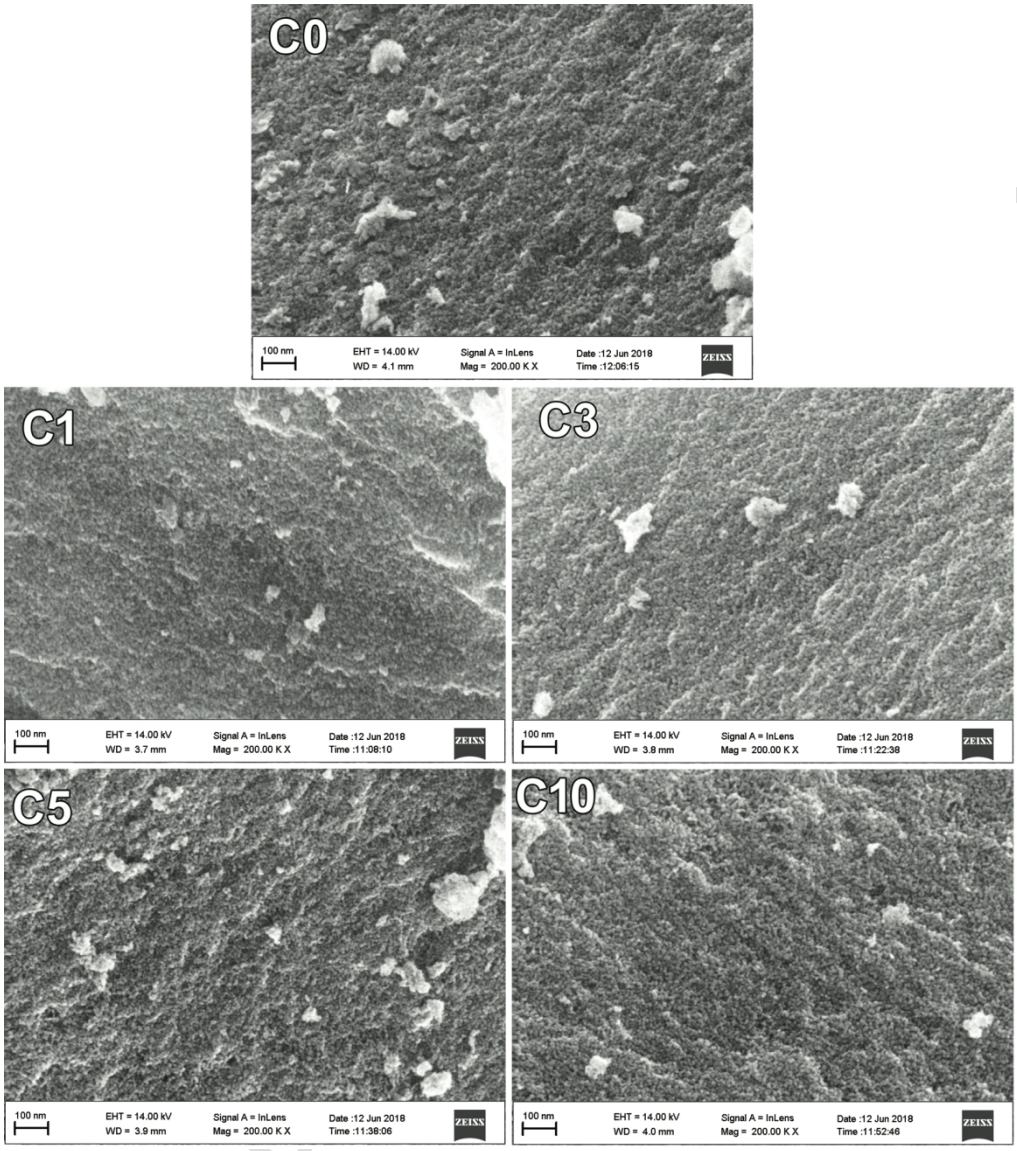

Fig.4 FESEM images of NiO and Co doped NiO nanoparticles

The chemical compositions of the synthesized NiO nanoparticles doped with different *Co* concentrations are measured by EDX spectra, are shown in Fig. 5. The patterns confirm the presence of *Ni, O* and *Co* as the only elementary species in the sample. No additional peaks corresponding to any other elements are observed. Hence the synthesized materials are pure and without any contamination. The result of EDX analysis matches with the doping percentage, and is presented in Table 2.

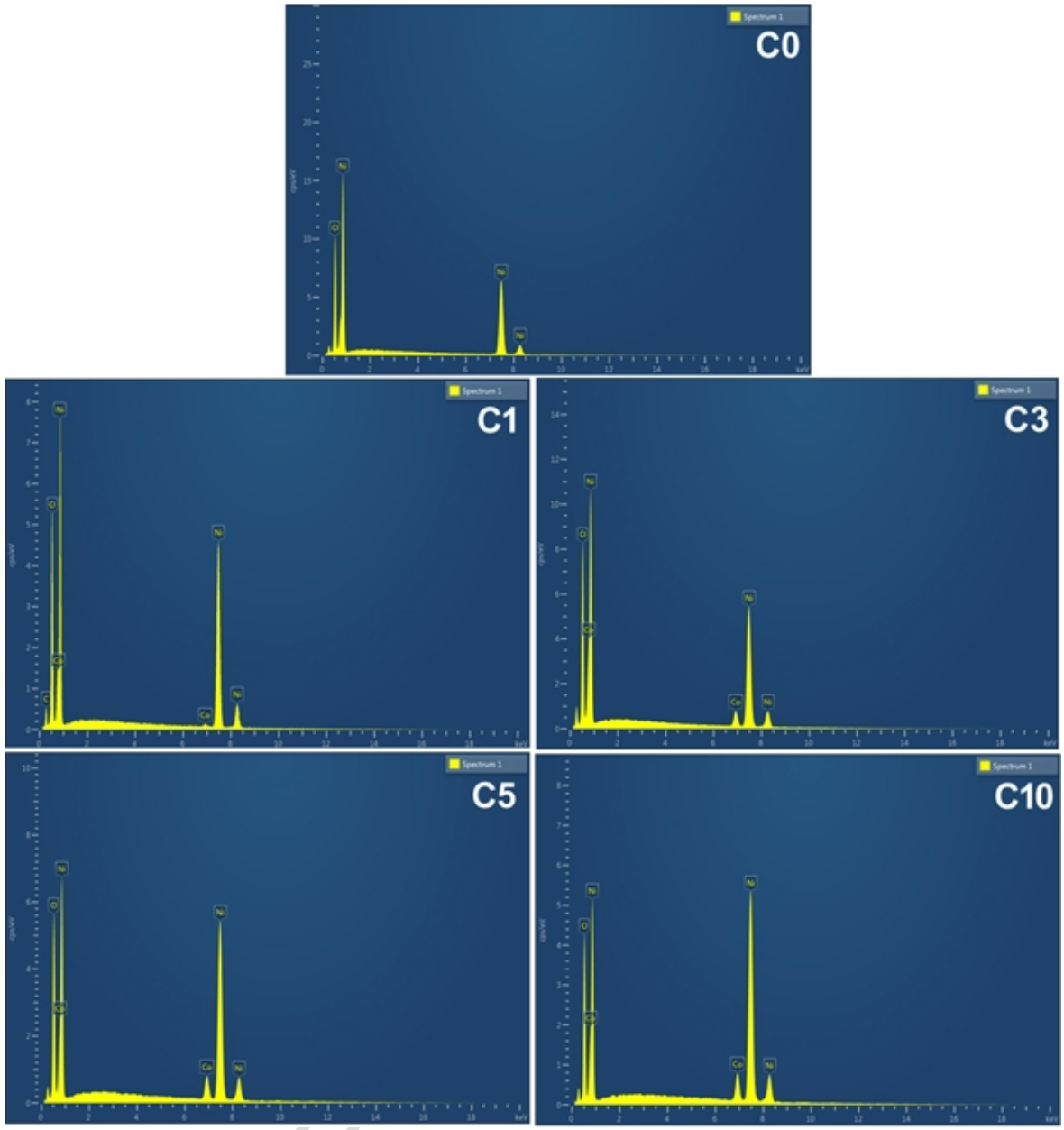

Fig.5. Chemical composition of NiO and *Co* doped NiO nanoparticles

Table 2. Chemical composition of the samples

	Atomic percentage		
Sample	**Ni**	**O**	**Co**
S0	39.25	60.75	0
C1	40.97	58.43	0.6
C3	61.52	36.26	2.22
C5	52.01	44.2	3.79
C10	48.57	43.89	7.54

3.3.2 TEM

TEM analysis is done to further elucidate the morphology and nanostructure of the samples. TEM bright field images, HRTEM images and selected area electron diffraction (SAED) patterns of all the samples are portrayed in Fig. 6. TEM images reveal that the particles are not spherical in shape. The average particle size of C0, C1, C3, C5 and C10 samples are measured to be 11.4, 9.9, 8.1, 9.5 and 9 nm respectively. HRTEM images show fringe pattern for all the samples. SAED patterns taken for pristine and *Co* doped samples show clear spots arranged in ring shape corresponding to different planes of NiO. The patterns confirm the crystalline nature and phase purity of the samples. Table 3 gives the structural parameters of the samples obtained from TEM images.

Table 3. Geometrical parameters of the samples from TEM images

Sample	**Average particle size from TEM images (nm)**	**d spacing from HRTEM images (nm)**	**d spacing from SAED patterns (nm)**		
			(111)	**(200)**	**(220)**
C0	11.4±0.228	0.21 (200)	0.2856	0.2463	0.1745
C1	9.9±0.198	0.21(200)	0.2841	0.2462	0.1742
C3	8.1±0.162	0.17 (220)	0.2857	0.2435	0.1740
C5	9.5±0.19	0.16 (220)	0.2834	0.2418	0.1730
C10	9.0±0.18	0.21(200)	0.2790	0.2410	0.1719

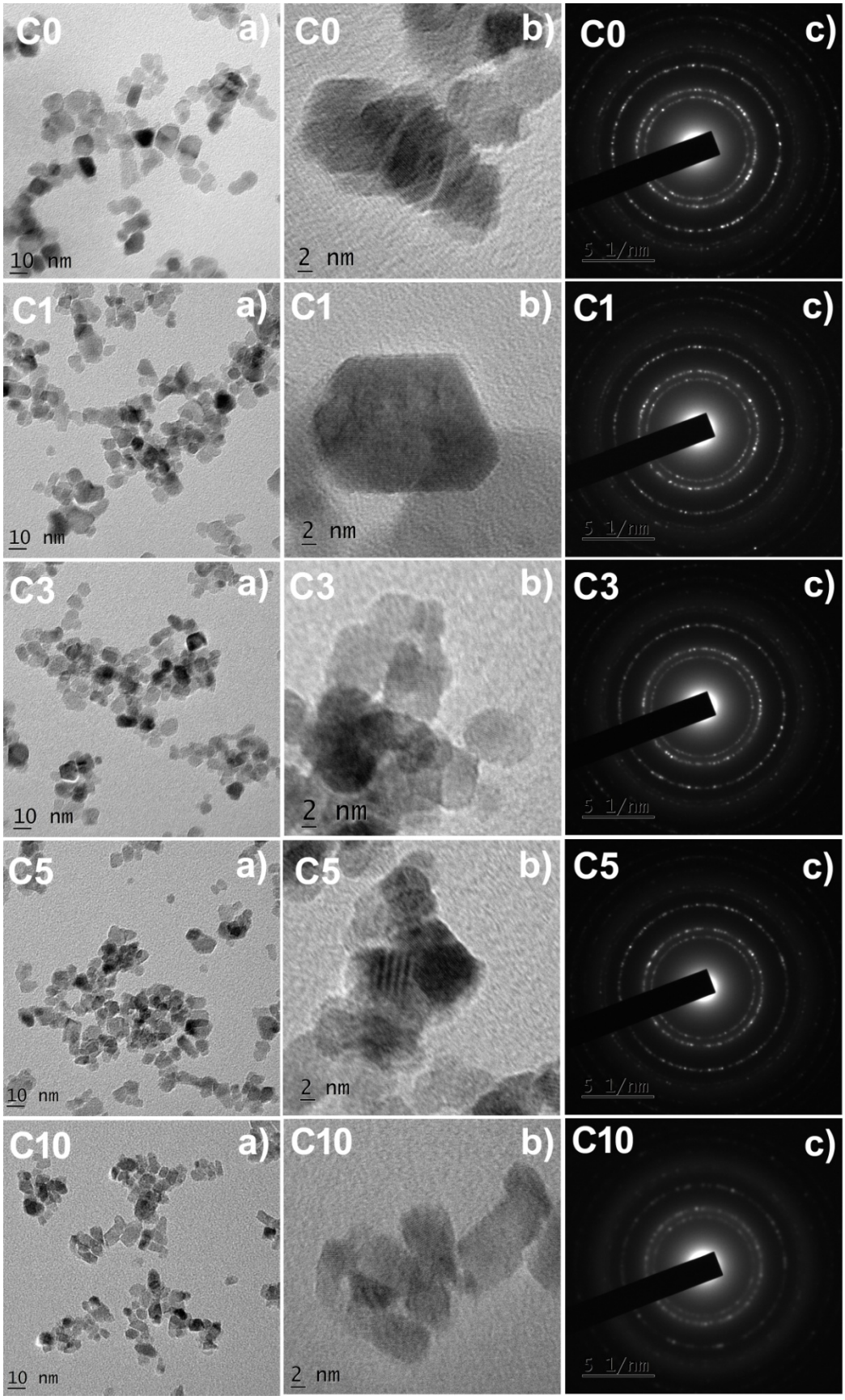

Fig.6 a) Bright field images, b) HRTEM images and c) SAED patterns of NiO and Co doped NiO nanoparticles

3.4 XPS Studies

XPS analysis aims to identify the oxidation states of the constituent ions present in the sample. The XPS wide spectra of all the samples are shown in Fig. 7a. The characteristic peaks corresponding to *Ni, O* and *Co* observed in the spectrum of all doped samples confirm the compositional purity of the samples. Slight shift in the binding energies to higher values is observed, which can be ascribed to *Co* doping. Fig.7 (b-d) shows the core level spectrum of *Ni, O* and *Co* respectively in sample C3. The *Ni 2p* spectrum exhibits the characteristic double peaks for $2p_{3/2}$ and $2p_{1/2}$ main lines. The peaks at binding energies 853.4 and 855.2 eV correspond to $Ni2p_3$A and $Ni2p_3$B and those at 870.9 and 878.8 eV to $Ni2p_1$A and $Ni2p_1$B respectively. The extra peak at high binding energy indicates the presence of small amount of Ni^{3+} along with the Ni^{2+} states [33, 34]. Due to shake up process, the satellite peaks appear at 860.7 eV ($Ni2p_3$) and 878.8 eV ($Ni2p_1$) respectively [35]. The *Ni2p* spectrum matches well with the reported XPS peak positions and shapes. The high resolution *O 1s* spectra can be resolved into two components at 529 and 530.9 eV which corresponds to *O 1s* core level of the O^{2-} anions in the sample and the adsorbed oxygen on the sample surface respectively. In the spectrum of cobalt, the peak at a binding energy of 778.95 eV corresponding to $Co2p_3$ confirm the presence of Co^{2+} ions in the sample [35, 36]

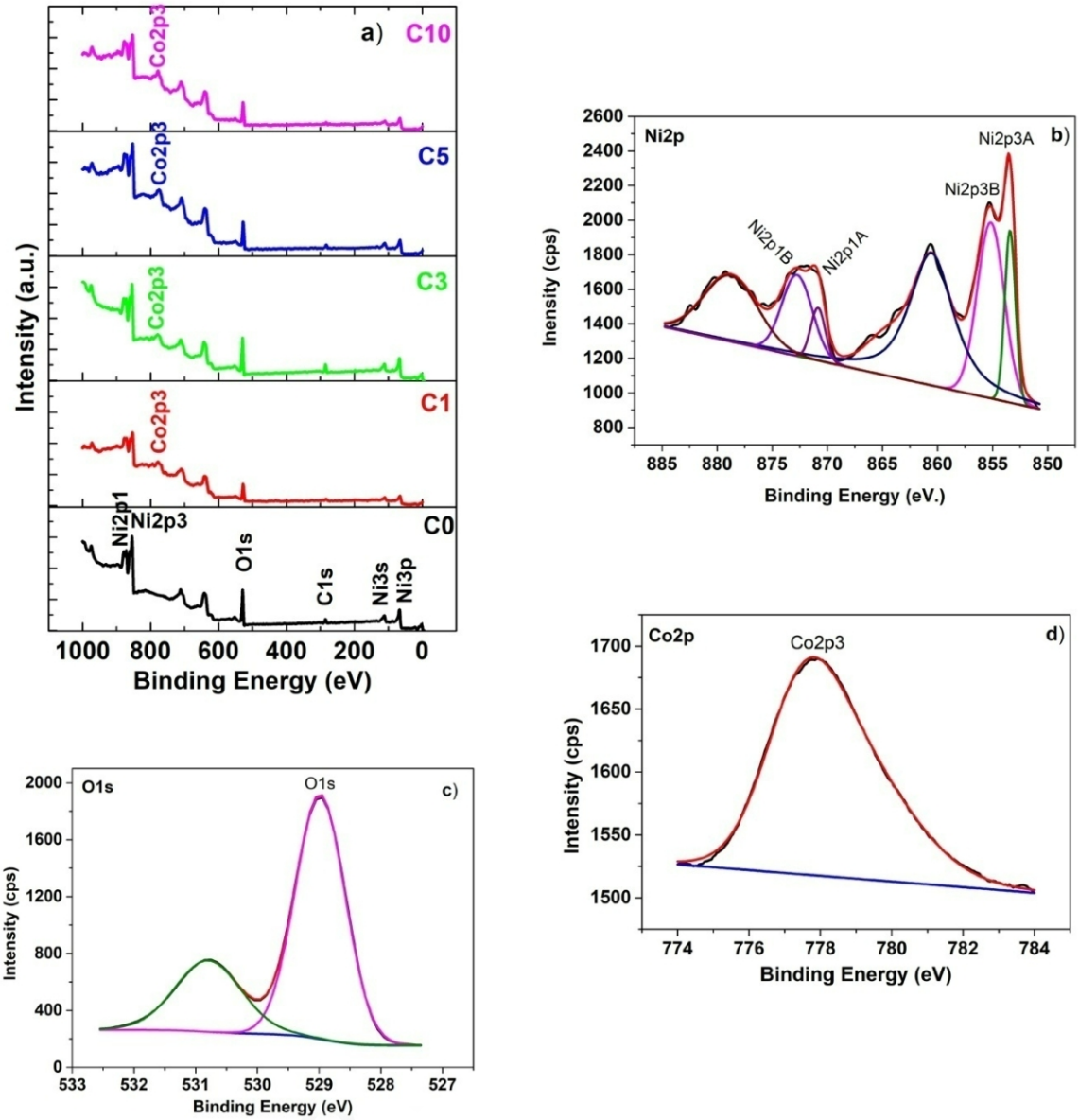

Fig.7. XPS spectra of a) all samples (wide scan), b) *Ni 2p*, c) *O 1s* and d) Co 2p

3.5 Optical Studies

3.5.1 UV- Visible

UV-visible absorption spectra of pure and doped samples of NiO nanoparticles are shown in Fig.8. All samples exhibit strong UV absorption along with extended visible light absorption. The UV absorption corresponds to the bandgap absorption of NiO. Pristine NiO has very good absorption in the entire visible range too. Absorption in the wavelength longer than 400 nm is due to the presence of excess oxygen in the lattice which is confirmed by the EDX data. This leads to the creation of Ni^{2+} vacancies and in order to acquire local charge compensation, two Ni^{3+} ions are produced. This change in the oxidation state of *Ni* is the reason for the featureless absorption in the visible region [37, 38]. This inference is consistent

with the XPS measurement. As the doping concentration increases, broad absorption in the visible region decreases which may be due to the change in stoichiometry as evident from the EDX data. The absorption becomes more selective, with the samples C5 and C10 having a hump in the 350 – 500 nm range. This is due to the ligand to dopant ($O^{2-} \rightarrow Co^{2+}$) charge transfer [39]. The intensity of the *Co* related peak is found to increase with increase in dopant concentration.

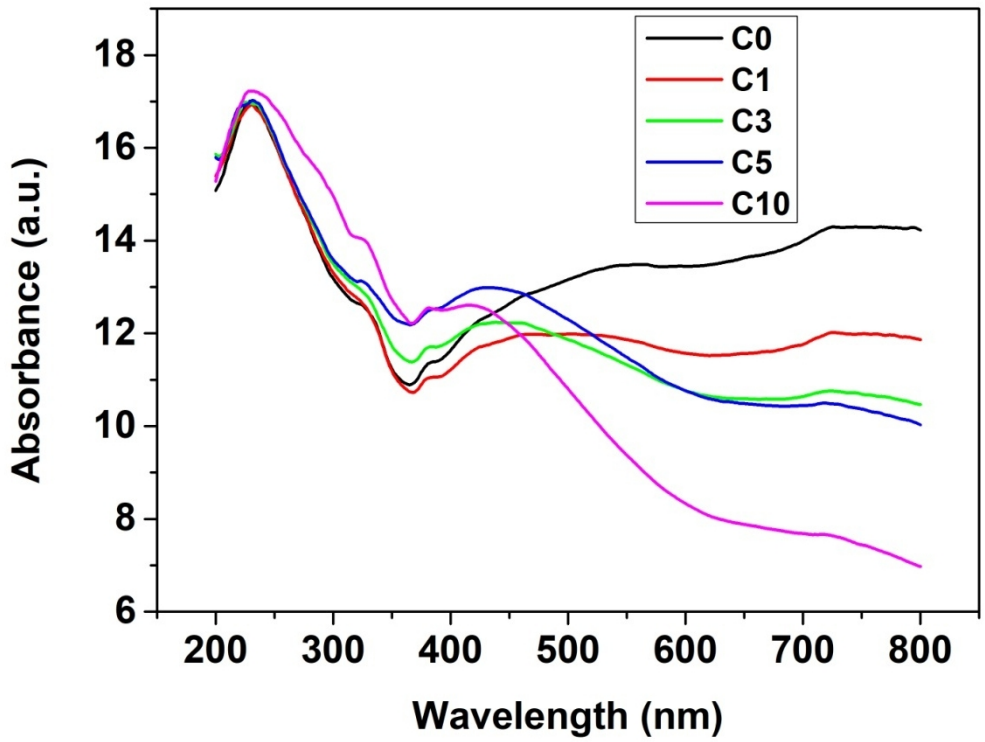

Fig.8 UV – visible absorption spectra of NiO and *Co* doped NiO nanoparticles

The pristine *NiO* sample has the absorption edge at 347 nm which is found to get slightly red shifted with increase in doping concentration. The optical bandgap values determined from the hν - $(\alpha h\nu)^2$ graph (Fig.9) for C0, C1, C3, C5 and C10 are 3.71, 3.65, 3.58, 3.56 and 3.24 eV respectively. The energy bandgap of NiO exists between the *O 2p* states of the valence band and *Ni 3d* states of the conduction band. The decrease in the optical bandgap on *Co* doping is due to the structural modifications of NiO. Since the XRD data show no obvious structural changes, local structural modifications surrounding the *Co* dopant atoms may play a key role in the mechanism underlying the observed bandgap narrowing. Doping introduces oxygen vacancies, which is clear from the EDX data. According to XPS results, cobalt exists in Co^{2+} oxidation state in the sites occupied by cations in the host lattice [15]. Such *Co* ions and oxygen vacancies introduce some additional energy levels in the NiO

bandgap near the valence band edge. Consequently, the absorption edge transition for the doped material can be from *O 2p* to *Co 3d* state which leads to the decreased optical bandgap [10]. The increased sp-d exchange interactions between the band electrons and the localized d electrons of Co^{2+} cations also contribute to bandgap narrowing [40]. Therefore, the sub-band states of Co^{2+} and the oxygen vacancy states are responsible for the reduction of effective bandgap of NiO nanoparticles. As the doping concentration increases, the defect levels go deep into the band gap which further reduces the bandgap. Thus the bandgap of NiO can be reduced considerably by *Co* doping without causing any significant structural modifications, which makes them useful for various optoelectronic applications.

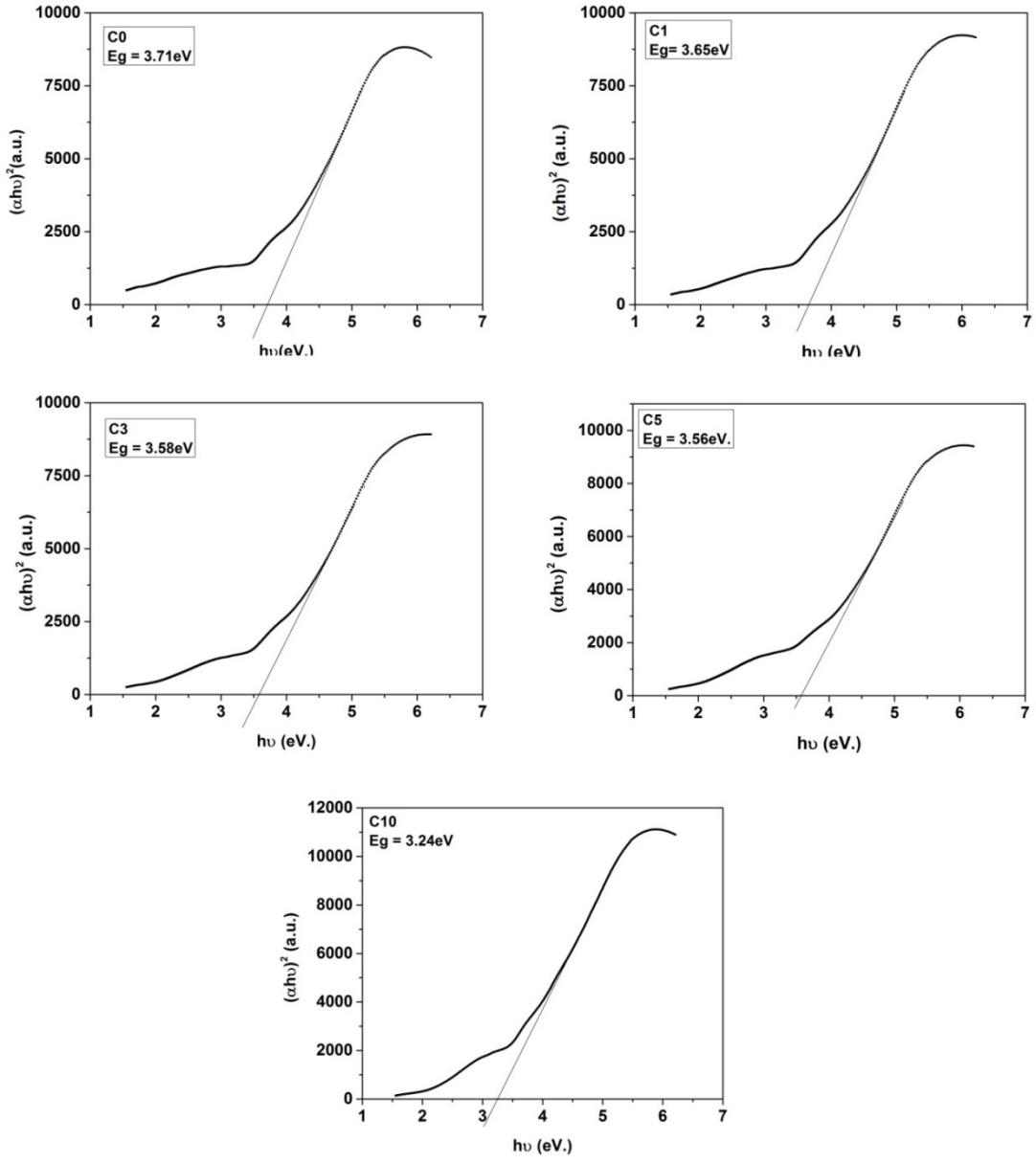

Fig.9 Tauc plots of NiO and *Co* doped NiO nanoparticles

3.5.2 PL Analysis

The room temperature PL spectra of pure and *Co* doped NiO samples excited at a wavelength of 280 nm are shown in Fig.10. Strong UV emission centred at 380 nm (3.26 eV) is observed along with well-resolved shoulder peaks at 447 nm (2.78 eV), 465 nm (2.67 eV), 490 nm (2.53 eV) and 512 nm (2.43 eV). The shoulder peaks corresponding to violet, blue and green emissions might be ascribed to defect states such as nickel vacancies, oxygen vacancies and nickel interstitials. This wide range of emission extending from UV to the visible region originates from the defect levels of NiO nanoparticles. It is reported that the UV emission due to excitonic recombination corresponds to the near band edge emission of NiO [41]. The shoulder peaks in the visible region originate from the radiative recombination of photo-generated holes with electrons occupying the surface oxygen vacancies and defects [42].

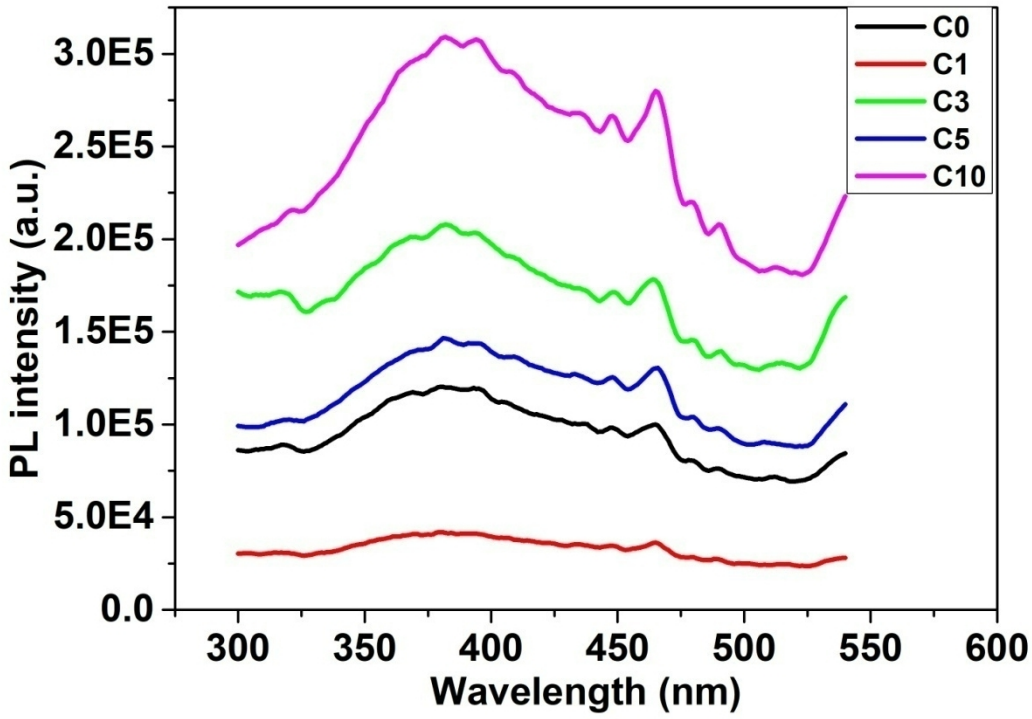

Fig.10 PL spectra of NiO and *Co* doped NiO nanoparticles

Co doping does not give rise to new emission compared to that of undoped NiO, however, it has a great effect on the PL intensity. 1 mol % of *Co* doping led to a significant decrease in the emission intensity compared with that of pure NiO. The quenching of PL intensity confirms that an appropriate amount of *Co* doping inhibits the recombination rate of

photo generated electron–hole pairs. The PL intensity of C3, C5 and C10 samples are higher than that of pure NiO. The increase in the surface oxygen vacancies and defects, as evident from the EDX data can enhance the PL intensity of the doped samples. The levels corresponding to oxygen vacancies and defects in the bandgap bind the photo-induced electrons easily to form excitons, which makes the PL emission easy [43]. As the doping concentration increases, the dopant levels introduced in the energy gap can also act as recombination centers of photo-generated electron–hole pairs which in turn enhance the PL intensity. PL intensity for sample C3 is higher than that of C5, which may be due to smaller particle size. The decrease in particle size may also lead to an increase in oxygen vacancies which in turn enhances the PL intensity [44]. This is the first report on the enhancement of PL intensity with *Co* doping of NiO nanoparticles. The PL emission results are in good agreement with EDX and UV-Visible studies. Thus the PL emission studies of NiO with varying *Co* concentration, is an efficient method for the exploration of point defects such as oxygen/nickel vacancies and interstitials in the host lattice. In short, results of the optical studies confirm that doping with *Co* can be used to tune optical properties such as bandgap values and PL intensity of NiO nanoparticles for potential optoelectronic applications.

4. Conclusion

$Ni_{1-x}Co_xO$ (x= 0, 0.01, 0.03, 0.05 and 0.10) nanoparticles are successfully prepared by a co-precipitation method. No evidence of secondary phases is found in the XRD pattern which indicates that the *Co* dopant get substituted at the *Ni* site without changing the cubic structure. The W-H plot shows an increase in microstrain with doping. Compositional analysis (EDS and XPS) ascertained the existence of only *Ni*, *O*, and *Co* in the synthesized samples. The PL intensity is found to vary considerably with *Co* doping. The red shift in the absorption edge and the reduction in bandgap of NiO with increase in *Co* doping concentration indicate the presence of oxygen vacancies at the nickel interstitials. In brief, the tuning of bandgap and PL intensity by *Co* doping of suitable concentrations makes NiO nanoparticles competent for various optoelectronic applications.

Acknowledgements

The authors acknowledge Nirmala College, Muvattupuzha and Newman College, Thodupuzha for providing the facilities to conduct this study. They are also grateful to SAIF Cochin and Amrita centre for nanosciences, Ernakulam for the technical support rendered. The first author acknowledges University Grants Commission for facilitating the research work through FDP.

References

[1] M. El-Kemary, N. Nagy, I. El-Mehasseb, Materials Science in Semiconductor Processing 16 (2013) 1747–1752

[2] D. Adler, J. Feinleib, Electrical and optical properties of narrow-band materials, Phys.Rev.B2 (1970) 3112–3134

[3] M. Kitao, K. Izawa, K. Urabe, T. Komatsu, S. Kuwano, S. Yamada, Preparation and Electrochromic Properties of RF-Sputtered NiO_x Films Prepared in $Ar/O_2/H_2$ Atmosphere, Jpn. J. Appl. Phys. 33 (1994) 6656.

[4] Y. Du, W. Wang, X. Li, J. Zhao, J. Ma, Y. Liu, G. Lu, Preparation of NiO nanoparticles in microemulsion and its gas sensing performance, Mater. Lett. 68 (2012) 168–170

[5] X. Wan, M. Yuan, S. Tie, S. Lan, Effects of catalyst characters on the photocatalytic activity and process of NiO nanoparticles in the degradation of methylene blue, Appl. Surf. Sci. 277 (2013) 40– 46

[6] M. P. Proenca, C. T. Sousa, A. M. Pereira, P. B. Tavares, J. Ventura, M. Vazquez, J. P. Araujo, Size and surface effects on the magnetic properties of NiO nanoparticles, Phys. Chem. Chem. Phys.,13 (2011) 9561–9567

[7] F. Li, H.Chen, C.Wang, K. Hu, A novel modified NiO cathode for molten carbonate fuel cells, J. Electroanal. Chem.531(2002) 53 – 60

[8] A. Nattestad, M. Ferguson, R. Kerr, Y.B. Cheng, U. Bach, Dye-sensitized nickel (II)oxide photocathodes for tandem solar cell applications, Nanotechnology 19 (2008) 295304

[9] N. Alidoust, M.C. Toroker, J. A. Keith, E. A. Carter, Significant reduction in NiO band gap upon formation of $Li_x Ni_{1-x} O$ alloys : applications to solar energy conversion, ChemSusChem, 7 (2014) 195 – 201

[10] B. Sahin, F. Bayansal, M. Yüksel, H.A. Çetinkara, Influence of annealing to the properties of un-doped and Co-doped CdO films, Mater. Sci. Semicon. Proc. 18 (2014) 135 – 140

[11] A. Chanda, S. Gupta, M. Vasundhara, S. R. Joshi, G. R. Mutta, J. Singh, Study of structural, optical and magnetic properties of cobalt doped ZnO nanorods, RSC Adv.,7(2017) 50527–50536

[12] M. J. Chithra, K. Pushpanathan, M. Loganathan, Structural and Optical Properties of Co-Doped ZnO Nanoparticles Synthesized by Precipitation Method, Mater. Manuf. Processes, 29(2014) 771–779

[13] R.D. Shannon, Revised Effective Ionic Radii and Systematic Studies of Interatomie Distances in Halides and Chaleogenides, Acta Cryst. A 32 (1976) 751- 767

[14] G. Natu, P. Hasin, Z. Huang, Z. Ji, M. He, Y. Wu, Valence Band-Edge Engineering of Nickel Oxide Nanoparticles via Cobalt Doping for Application in p-Type Dye-Sensitized Solar Cells, ACS Appl. Mater. Interfaces 4 (2012) 5922-5929

[15] T.Taşköprü, F.Bayansal, B. Şahin, M. Zor, Structural and optical properties of Co-doped NiO films prepared by SILAR method, Philos.Mag.95 (2014) 32–40

[16] S. Agrawal, A. Parveen, A. Azam, Microwave assisted synthesis of Co doped NiO nanoparticles and its fluorescence properties. J. Lumin. 184, (2017) 250-255

[17] P. Mallick, C.S. Sahoo, N.C. Mishra, Structural and Optical Characterization of NiO nanoparticles synthesized by sol-gel route. AIP Conf. Proc., 1461 (2012) 229-232.

[18] A.K. Mishra, S. Bandyopadhyay, D. Das, Structural and magnetic properties of pristine and Fe-doped NiO nanoparticles synthesized by the co-precipitation method, Mater. Res. Bull. 47 (2012) 2288–2293

[19] S. Takami, R. Hayakawa, Y. Wakayama, T. Chikyow, Continuous hydrothermal synthesis of nickel oxide nanoplates and their use as nanoinks for p-type channel material in a bottom-gate field-effect transistor. Nanotechnol, 21, (2010)134009 doi: 10.1088/0957-4484/21/13/134009.

[20] K. Anandan, V. Rajendran, Morphological and size effects of NiO nanoparticles via solvothermal process and their optical properties. Mater. Sci. Semicond. Process, 14, (2011) 43 – 47

[21] P.A.Sheena, K.P. Priyanka, N.A. Sabu, S. Ganesh, T. Varghese, Effect of electron beam irradiation on the structure and optical properties of nickel oxide nanocubes, Bull. Mater. Sci.,38 (2015) 825–830.

[22] V. Biju, M. Abdul Khadar, Analysis of AC electrical properties of nanocrystalline nickel oxide. Mater.Sci. Eng., A, 304-306 (2001) 814 – 817

[23] B. L. Cushing, V. L. Kolesnichenko, C. J. O'Connor, Recent Advances in the Liquid-Phase Syntheses of Inorganic Nanoparticles, Chem. Rev.,104 (9) (2004) 3893–3946

[24] P.A. Sheena, K.P. Priyanka, N. A. Sabu, B. Sabu, T. Varghese, Effect of calcination temperature on the structural and optical properties of nickel oxide nanoparticles, Nanosystems: Phys. Chem. Math. 5 (2014) 441- 449

[25] M. Alagiri, S. Ponnusamy, C. Muthamizhchelvan, Synthesis and characterization of NiO nanoparticles by sol–gel method, J Mater Sci: Mater Electron 23 (2012) 728–732

[26] P.M. Ponnusamy, S. Agilan, N. Muthukumarasamy, M. Raja, D. Velauthapillai, Studies on cobalt doped NiO nanoparticles prepared by simple chemical method, J. Mater. Sci.- Mater. Electron. 27 (2016) 399 - 406

[27] B.D. Cullity, Elements of X-Ray Diffraction, Addison-Wesley, Reading, MA (1967)

[28] R. Sharma, A.D. Acharya, S. Moghe, S.B. Shrivastava, M. Gangrade, T. Shripathi, V. Ganesan, Effect of cobalt doping on microstructural and optical properties of nickel oxide thin films, Mater. Sci. Semicond. Process. 23 (2014) 42

[29] G.K. Williamson, W.H. Hall, X-ray line broadening from filed aluminum and wolfram. Acta Metall. 1(1953) 22-31

[30] D.N. Srivastava, V.G. Pol, O. Palchik, L. Zhang, J.C. Yu, A. Gedanken, Preparation of stable porous nickel and cobalt oxides using simple inorganic precursor, instead of alkoxides, by a sonochemical technique, Ultrason Sonochem. 12 (2005) 205 – 212

[31] L. Wu, Y. Wu, H. Wei, Y. Shi, C. Hu, Synthesis and characteristics of NiO nanowire by a solution method, Mater. Lett. 58 (2004) 2700 – 2703

[32] A.C.Tas, P.J.Majewski, F.Aldinger, Synthesis of Gallium Oxide Hydroxide Crystals in Aqueous Solutions with or without Urea and Their Calcination Behavior, J.Am.Ceram.Soc., 85(2002)1421- 1429

[33] M.A. van Veenendaal, G.A. Sawatzky, Nonlocal screening effects in 2*p* x-ray photoemission spectroscopy core-level line shapes of transition metal compounds, Phys. Rev. Lett. 70 (1993) 2459 – 2462

[34] L. Cao, D. Wang, R. Wang, NiO thin films grown directly on Cu foils by pulsed laser deposition as anode materials for lithium ion batteries, Mater. Lett. 132 (2014) 357 - 360.

[35] T. V. Thi, A. K. Rai, J. Gim, J. Kim, High performance of Co-doped NiO nanoparticle anode material for rechargeable lithium ion batteries, Journal of Power Sources 292 (2015) 23 – 30

[36] A. A. Jacob, L. Balakrishnan, K. Shambavi , Z. C. Alex, Multi-band visible photoresponse study of Co^{2+}doped ZnO nanoparticles, RSC Adv., 2017, 7, 39657–39665

[37] A. Mendoza-Galvan, M. A. Vidales-Hurtado, A. M. Lopez Beltran, Comparison of the optical and structural properties of nickel oxide-based thin films obtained by chemical bath and sputtering, Thin Solid Films, 2009, 517, 3115–3120

[38] G. Madhu, V.Biju, Effect ofNi^{2+} and O^{2-} vacancies on the electrical and optical properties of nanostructured nickel oxide synthesized through a facile chemical route, Physica E60 (2014) 200–205

[39] M. Salavati-Niasari, A Khansari, F. Davar, Synthesis and characterization of cobalt oxide nanoparticles by thermal treatment process, Inorganica Chimica Acta, 362 (2009) 4937–4942

[40] R. He, R.K. Hocking, T. Tsuzuki , Co- doped ZnO nanopowders: Location of cobalt and reduction in photocatalytic activity, Mater. Chem. Phys.,132 (2012) 1035–40.

[41] L. Kumari, W.Z. Li, C.H. Vannoy, R.M. Leblanc, D.Z. Wang, Vertically aligned and interconnected nickel oxide nanowalls fabricated by hydrothermal route, Crystal Research and Technology 44 (2009) 495–499

[42] S.A. Makhlouf, M.A. Kassem, M.A. Abdel-Rahim, Crystallite size dependent optical properties of nanostructured NiO films, Optoelectron. Adv. Mater. 4 (2010) 1562.

[43] M. M. Khan, S. A. Ansari, D. Pradhan, M. O. Ansari, D. H. Han, J. Lee, M. H. Cho, Band gap engineered TiO_2 nanoparticles for visible light induced photoelectrochemical and photocatalytic studies, J. Mater. Chem. A, 2014, 2, 637–644

[44] J. Liqiang, S. Xiaojun, X. Baifu, W. Baiqi, C. Weimin, F. Honggang, The preparation and characterization of La doped TiO2 nanoparticles and their photocatalytic activity, J. Solid State Chem. 177 (2004) 3375 –3382

HIGHLIGHTS

- Particle size modulation and increase in microstrain on doping of *NiO* with Co^{2+}ions
- Tuning of bandgap on doping
- Emission bands give an insight into the defect structure
- First report on the enhancement of PL intensity with *Co* doping of *NiO*
- First comprehensive report for the characterization of *Co* doped of *NiO* nanoparticles

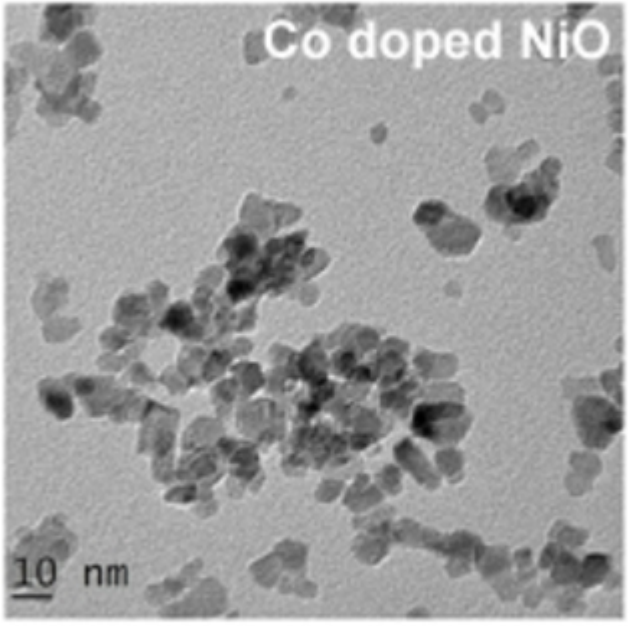
Co doped NiO
10 nm

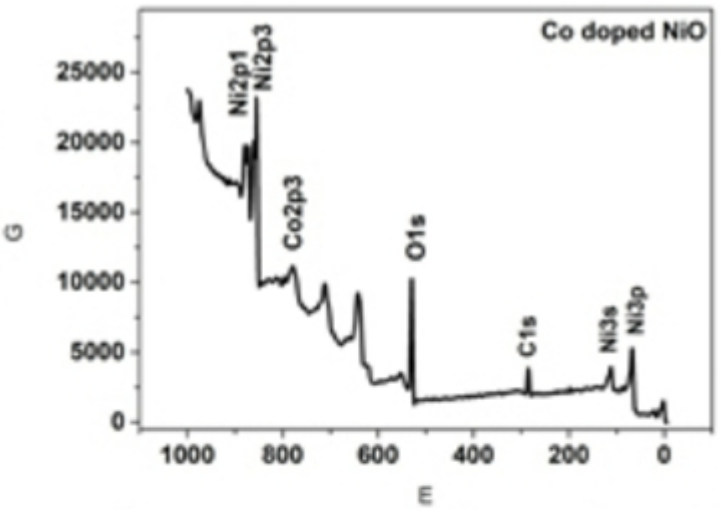
Co doped NiO
Ni2p1
Ni2p3
Co2p3
O1s
C1s
Ni3s
Ni3p
G
E
25000
20000
15000
10000
5000
0
1000
800
600
400
200
0

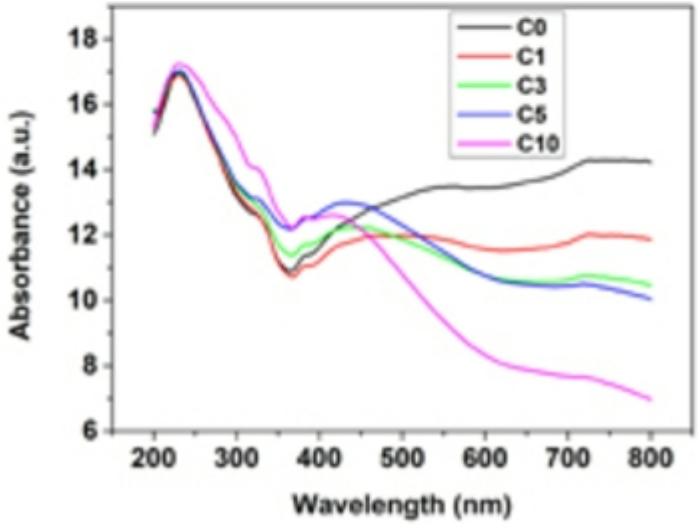
C0
C1
C3
C5
C10
Absorbance (a.u.)
Wavelength (nm)
18
16
14
12
10
8
6
200
300
400
500
600
700
800